JGR Oceans

RESEARCH ARTICLE
10.1029/2019JC015415

Arctic Ocean Precipitation From Atmospheric Reanalyses and Comparisons With North Pole Drifting Station Records

Andrew P. Barrett[1], **Julienne C. Stroeve**[1,2], **and Mark C. Serreze**[1]

[1]National Snow and Ice Data Center, University of Colorado at Boulder, Boulder, CO, USA, [2]University College London, Earth Sciences, London, UK

Key Points:
- Arctic Ocean precipitation from six global atmospheric reanalyses is compared against measured precipitation
- All reanalyses capture known spatial and seasonal patterns of precipitation but differ in the amount of precipitation
- Time series of annual precipitation over the central Arctic Ocean from the six reanalyses are strongly correlated with each other

Supporting Information:
- Supporting Information S1

Correspondence to:
A. P. Barrett,
apbarret@nsidc.org

Citation:
Barrett, A. P., Stroeve, J. C, & Serreze, M. C. (2020). Arctic Ocean precipitation from atmospheric reanalyses and comparisons with North Pole drifting station records. *Journal of Geophysical Research: Oceans, 125*, e2019JC015415. https://doi.org/10.1029/2019JC015415

Received 24 JUN 2019
Accepted 26 DEC 2019
Accepted article online 9 JAN 2020

Abstract We evaluate fields of Arctic Ocean precipitation from six atmospheric reanalyses: NASA MERRA, NASA MERRA2, NOAA CFSR/CFSv2, ECMWF ERA-Interim, ECMWF ERA5, and JMAO JRA55. The study is motivated by recognition that precipitation fields from reanalyses can serve as the key input into snow on sea ice accumulation models, supporting retrievals of sea ice thickness from satellite altimeter systems. Time series of annual precipitation over the central Arctic Ocean correlate well between all reanalyses, and they all capture the basic spatial and seasonal patterns of Arctic precipitation. However, they differ strongly with respect to precipitation amount: CFSR and MERRA2 are wetter than the other reanalyses. All reanalyses depict that the majority of total annual precipitation over the central Arctic Ocean comes from small events, less than 1 mm/day. Validation is challenged by sparse observations, uncertain adjustments for gauge undercatch, and other issues. However, given that correlations with data from Russian North Pole drifting station records are all roughly equal and that they depict similar interannual variability at the regional scale, all of the reanalyses appear suitable for supporting retrievals of ice thickness (provided that appropriate bias corrections can be applied). However, only CFSR, MERRA2, ERA5, and JRA55 will continue to generate output beyond 2019.

Plain Language Summary While the thickness of the sea ice that floats atop the Arctic Ocean can be measured using satellite altimeters—instruments that measure the height that something projects above the surface—this assumes that one knows the mass of any snow cover that lies atop the ice. Estimating the overlying snow cover is a formidable task. One way forward is to use estimates of precipitation from a type of weather model known as an atmospheric reanalysis. We look at precipitation from six different reanalyses and find that all of them hold much potential for providing fields of precipitation.

1. Introduction

Retrievals of sea ice thickness over the Arctic Ocean from satellite altimeter systems such as CryoSat-2 (a radar system) and ICESat-2 (a laser system) critically depend on knowledge of the overlying snow cover. Satellite altimeters do not provide direct estimates of ice thickness but instead return the height of the snow or ice surface above a reference ellipsoid. This height is converted to the height of the snow or ice surface above the local sea surface—the freeboard. Where ice is snow covered, information on snow depth and density (allowing for estimation of the mass of snow) is needed to convert this freeboard into ice thickness (Giles et al., 2007; Kwok, 2010). However, direct measurements of snow cover and precipitation (which can be used along with other variables to estimate snow cover) are sparse and cannot provide the needed gridded time series. Alternative approaches are required.

There is potential to retrieve snow depth using satellite passive microwave brightness temperatures. Retrievals are generally limited to first-year ice (Markus et al., 2011), although efforts to extend approaches over multiyear ice regions have been offered (Rostosky et al., 2018). Combinations of freeboard estimates from Ku (~12 GHz) and Ka (~37 GHz) band radar altimeters, which reflect from snow-ice and atmosphere-ice interfaces, respectively, also provide potential for snow thickness retrievals, with root-mean-square errors up to 7.6 cm (Lawrence et al., 2018). However, radar penetration is dependent on snow salinity, adding uncertainty to snow depth estimates (Nandan et al., 2017). Combinations of radar and LIDAR likely suffer from similar problems. A further shortcoming of these satellite-based approaches is that density still has to be estimated to obtain snow mass. Drifting snow and ice mass balance buoys can provide

information on precipitation, as well as direct estimates of snow depth. Boisvert et al. (2018) compared the frequency of snowfall events and accumulated snowfall with snow depth measured by ice mass balance buoys. However, accumulated snow depth from these systems cannot be directly compared with precipitation because snow depths are influenced by deposition and erosion by wind. Precipitation histories must be "retrieved" from snow accumulation histories.

A particularly attractive option is to use estimates of precipitation, snowfall, near-surface air temperature, and other meteorological variables from atmospheric reanalyses to drive snow accumulation models. For example, Kwok and Cunningham (2008) simulated fields of snow thickness using temperature and precipitation output from the ERA-Interim reanalysis. Ice-covered grid cells were tracked as they moved across the Arctic Ocean, accumulating solid precipitation along their path. Petty et al. (2018) followed a similar approach, but with more sophistication by including two snow layers and parameterizations for wind packing and snow blowing into leads. Several reanalyses were tested to estimate snow depth and density between August and April, representing the period approximately spanning the start of the snow accumulation season to maximum sea ice extent. Simulating snow cover during the summer requires estimation of snow melt; Stroeve et al. (submitted to Journal of Geophysical Research) offer a path forward.

Estimation of snow accumulation over the Arctic Ocean from atmospheric reanalyses fundamentally depends on the quality of the input precipitation fields. Therefore, it is imperative to assess how well various reanalyses capture observed precipitation over the Arctic Ocean and its variability. Serreze et al. (2005) previously compared precipitation from the earlier generation ERA-40, ERA-15, and NCEP-R1 reanalyses and satellite-derived precipitation from the Global Precipitation Climatology Project (GPCP) merged version 2 (Huffman et al., 1997) to a gridded data set of gauge observations that included land stations and observations from the Russian North Pole (NP) drifting stations (described below). All of the reanalyses performed better than the satellite-derived GPCP product when compared to observations, with ERA-40 and ERA-15 performing better than NCEP-R1. Lindsay et al. (2014) evaluated precipitation and surface energy fluxes from NCEP-R1, NCEP-R2, the Twentieth Century Reanalysis, MERRA, ERA-Interim, and JRA25 in the Arctic region but did not use observations over the Arctic Ocean. They found more consistency between MERRA, ERA-Interim, and JRA25 than between the other products.

Several other studies examined precipitation specifically over the Arctic Ocean. Cullather and Bosilovich (2011) compared 7-day (synoptic) moving averages of MERRA precipitation with uncorrected gauge measured precipitation from the NP stations and found that MERRA produced 11% more precipitation. They also found that in 56% of observations, precipitation occurred in MERRA when the drifting stations reported no precipitation. Stroeve et al. (submitted to Journal of Geophysical Research) used MERRA2 and ERA-Interim within a snow model (Liston et al., 2018) to accumulate snow over sea ice and found that ERA-Interim snow depths were generally underestimated as compared with snow depths from Operation Ice Bridge, whereas those from MERRA2 tended to overestimate snow depth. The obvious caveat is that the Operation Ice Bridge estimates are themselves uncertain.

The present paper expands on previous studies by including and intercomparing newer reanalyses with a focus on the Arctic Ocean, and comparing the precipitation output against gauge-corrected precipitation estimates from the NP drifting stations. Specifically, we examine CFSR/CFSRv2, MERRA, MERRA2, ERA-Interim, ERA5, and JRA55. While it is known that there can be large differences between different reanalyses in precipitation, as well as strong biases with respect to observations (Bosilovich et al., 2011), these issues have not been adequately explored over the Arctic Ocean with a modern suite of reanalyses. Intercomparisons focus on the period 1980–2017 common to each reanalysis. This also spans the period of coverage of satellite and airborne altimeter missions that enable retrieval of sea ice and snow freeboards. Comparisons with the NP records cover the period 1979–1991 for which adjustments for gauge undercatch and other issues have been applied. Precipitation from the reanalyses is decomposed into wet day frequency (the number of days with recorded precipitation greater than 1 mm within a 24-h period), mean wet day frequency, and event size to understand whether differences arise from event frequency or amount. We examine results aggregated over an Arctic Ocean domain that encompasses the trajectories of the NP stations, spatial fields, and also make comparisons between individual monthly NP precipitation values and those from the reanalyses at the corresponding grid cells (Figure 1).

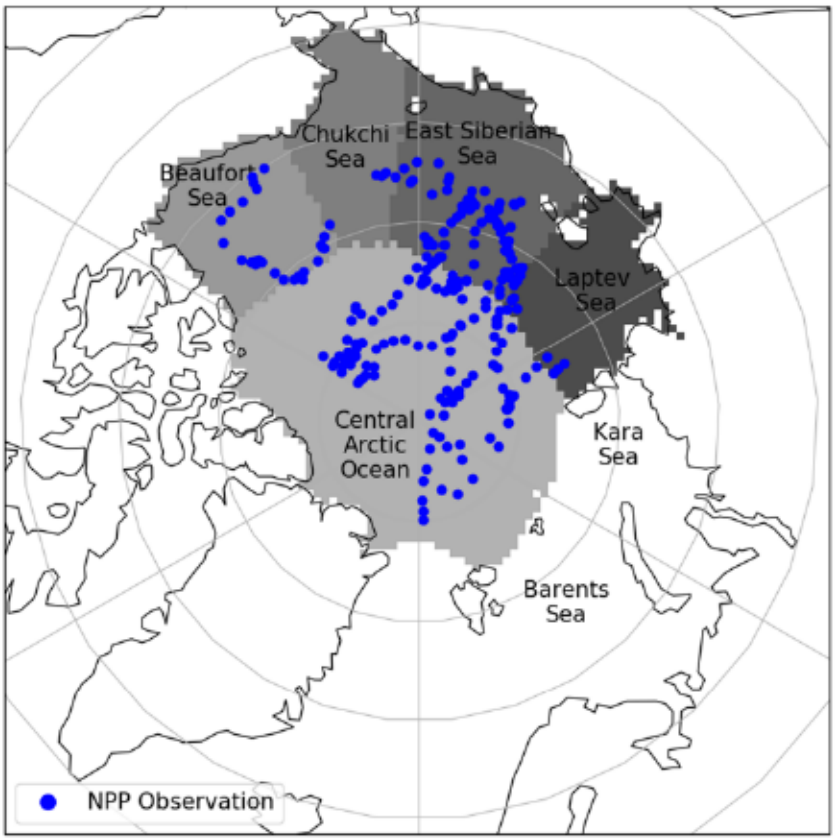

Figure 1. The Arctic Ocean domain and regions and mean monthly locations of the North Pole drifting stations.

2. Data and Methods

2.1. Atmospheric Reanalyses

An atmospheric reanalysis is a retrospective form of numerical weather prediction that uses a fixed version of a forecast model and data assimilation system. In an operational setting, the forecast model and data assimilation system are constantly refined to improve forecast accuracy, causing spurious nonclimatic "jumps" in archived fields. Reanalyses avoid this problem, yet they still suffer from nonclimatic jumps that result from changes in the amount, type, and quality of assimilation data.

Analyzed fields (analyses) such as geopotential height, air temperature, and humidity at standard atmospheric levels represent a blending of short-term forecasts with observations from radiosondes, satellites, aircraft reports, and other sources. This blending of forecasts with observations is performed during analysis cycles. These consist of the collection, selection and quality control of available observations, blending observations with a "first guess" or background forecast using an interpolation scheme to produce a new analysis, balancing the analysis to control fast-moving gravity waves, and integrating the forecast model forward in time to the beginning of the next analysis cycle, using the new analysis as initial conditions. The new forecast is the "first guess" for the next analysis. Forecasts of near-surface air temperature and humidity, surface fluxes, precipitation, and snowfall are also produced. Unlike analyses, these forecast fields are not directly influenced by observations and depend on parameterizations of subgrid-scale processes.

Numerical weather prediction in the Arctic is difficult, which bears on the quality of reanalyses in this area. Polar-orbiting environmental satellites provide a wealth of data, but assimilations are challenged by strong temperature inversions, persistent low cloud cover, and other issues. For example, based on comparisons with radiosonde profiles from Arctic coastal sites, Serreze et al. (2012) found that MERRA, CFSR, and ERA-Interim all have positive cold season humidity and temperature biases below the 850-hPa level and consequently do not capture observed low-level humidity and temperature inversions. This argues that

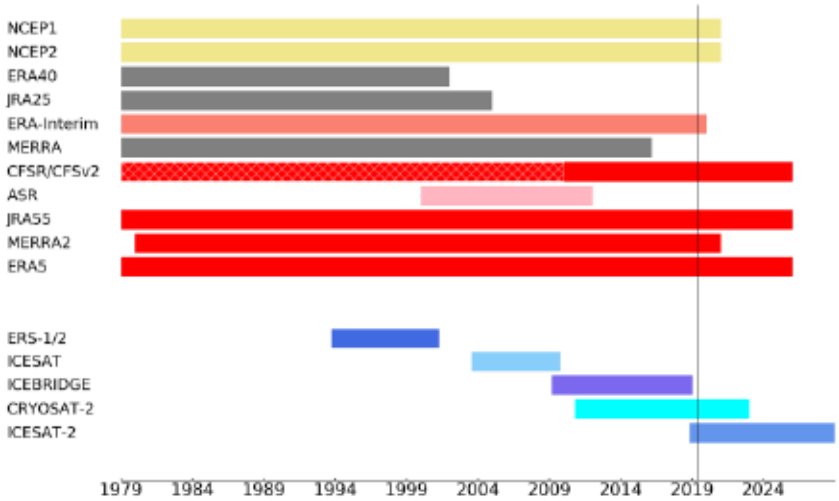

Figure 2. Production timelines of atmospheric reanalyses and operational lifetimes of satellite and airborne altimetry missions providing data for sea ice thickness retrievals. Crosshatching on the CFSR/CFSv2 timeline indicates the production period of CFSR.

low-level data from the radiosondes are often not being assimilated or are being given a low weight. In turn, the surface-based radiosonde network, while providing good coverage along the Arctic Ocean coast, offers little if any coverage over the central Arctic Ocean.

Figure 2 shows the production timelines for past and current reanalyses along with timespans of past and current altimeter missions: CryoSat-2 is expected to continue collecting data until December 2021, and ICESat-2 is expected to remain in operation for 5 to 7 years. Of the reanalyses, JRA55, MERRA2, CFSv2, and ERA5 are currently in production and will continue to be produced for the foreseeable future. ERA-Interim (the predecessor to ERA5) started production in 2006 and will be discontinued in 2019. ERA-Interim and MERRA provide a useful comparison with the reanalyses currently in production and furthermore span earlier altimeter missions (e.g., ICESat and ERS1/2). CFSR ended production in December 2010, but rather than producing a new reanalysis starting 1979, NCEP started CFSv2 in January 2011. CFSv2 is essentially the same forecast system as CFSR with a few minor changes and a higher spatial resolution. The original NCEP/NCAR reanalysis (NCEP-R1; the first reanalysis ever produced) and NCEP/DOE reanalysis (NCEP-R2), while still in production, are much older systems and hence are not used. ERA-40 ended August 2002 and JRA25 ended January 2014.

Table 1 summarizes key features of the reanalyses used in our study. There have been considerable improvements in spatial and vertical resolution, and in representation of the atmosphere since the release of NCEP-R1 in 1995. With the exception of MERRA and MERRA2, atmospheric fluid dynamic components of the forecast models (the dynamical cores) are represented in spectral space as a set of polynomial functions. For spectral models, model resolution is given as the wave number at which these functions are truncated; for example, T319 represents a truncation at wave number 319, with higher wave numbers indicating shorter wavelengths and therefore higher resolution. MERRA and MERRA2 use finite volume atmospheric fields discretized on a regular grid. All of the models have spatial resolutions better than 100 km, and in some cases (e.g., CFSv2 and ERA5) resolutions are similar to that of regional reanalyses. More vertical levels enable improved representation of atmospheric processes. The top levels for all of the included reanalyses extend into the mesosphere, allowing representation of upper atmosphere processes that influence the stratosphere and troposphere. By contrast, NCEP-R1 has a top level of 3 hPa.

Most reanalyses have used variational analysis as the framework for their statistical interpolation scheme. In variational analysis, the distance between the first-guess field and observations (the cost function) is minimized. MERRA, MERRA2, CFSR, and CFSv2 use 3D-Var. ERA-Interim, ERA5, and JRA55 use 4D-Var. In 3D-Var, the analysis is obtained by minimizing the distance between observations in the analysis time window and the first guess at the time of analysis. Observations further away in time from the analysis time may be excluded or weighted less than those closer to analysis time. The 4D-Var includes a time dimension and

Journal of Geophysical Research: Oceans

10.1029/2019JC015415

Table 1
Characteristics of the Seven Atmospheric Reanalyses Used in the Present Study

Model	MERRA	MERRA2	CFSR	CFSv2	ERA-I	ERA5	JRA-55
Model resolution[a]	½° lat. × ⅔° lon.	0.5° lat. × 0.625° lon.	T382 (~0.3° lat. × 0.3° lon.)	T574 (~0.2° lat. × 0.2° lon.)	T255 (0.75° lat. × 0.75° lon.)	T639 (0.3 lat. × 0.3° lon.)	T319 (~0.5° lat. × 0.625° lon.)
Output resolution	~55 km (37)	~55 km (35)	~38 km (17)	~23 km	~79 km (39)	~31 km (14)	~55 km (31)
Grid/model-type	Latitude-Longitude	Cubed-sphere	Spectral	Spectral	Spectral	Spectral	Spectral
Levels	72	72	64	64	60	137	60
Time span	1979–2011	1980 to present	1979–2010	2011 to present	1979 to present	1950 to present	1958 to present
Assimilation scheme	3D-Var/IAU	3D-Var/IAU	3D-Var	3D-Var	4D-Var	4D-Var	4D-Var
Bias correction	VarBC	VarBC	VarBC	VarBC	VarBC	VarBC[b]	VarBC
Humidity assimilated	Yes	Yes	Yes	Yes	In troposphere but not in stratosphere	Yes	Yes
Sea ice	Prescribed OISST	Prescribed CMIP/OISST/OSTIA	Assimilated	Assimilated	Prescribed NCEP (Grumbine, 1996)	Prescribed OSI-SAF	Prescribed COBE-SST[d]
Concentration threshold	50%		15% (fractional)	15% (fractional)	20% (fractional)	20% (fractional)	55% (binary)
Albedo	Fixed	Seasonal prescribed	Varies with surface	Varies with surface	Seasonal prescribed	Seasonal prescribed[c]	Function of solar zenith angle and T_{skin}
Reference	Rienecker et al. (2011)	Gelaro et al. (2017)	Saha et al. (2010)	Saha et al. (2013)	Dee et al. (2011)	https://climate.copernicus.eu/products/climate-reanalysis	Kobayashi et al. (2015)

[a]Resolution refers to spectral resolutions (numbers preceded by *T*) for all models except MERRA and MERRA2. Resolutions in brackets refer to grid spacing. [b]Variational bias correction applied to satellite irradiances, ozone, aircraft, surface pressure, and radiosondes (https://rda.ucar.edu/datasets/ds630.0/docs/ERA5.erai_era5_comparison.html). [c]Monthly values based on Ebert and Curry (1993) are interpolated to the forecast time. [d]Walsh and Chapman (2001) for Northern Hemisphere and climatology for Southern Hemisphere prior to 1978, microwave imager retrievals from Matsumoto et al. (2006) afterward.

aims to obtain an analysis that enables the best fit between observations and the evolution of the forecast through the analysis window. This approach allows better use of observations and improves forecasts (Talagrand, 2010). Fujiwara et al. (2017) provides a useful description of data assimilation approaches used in reanalyses. MERRA and MERRA2 include an additional step: the Incremental Analysis Update. In 3D-Var systems, analysis increments (the difference between first-guess and analysis fields) are added to the first-guess field before forecasts are made. This can cause unstable behavior in the model, in particular, a "spindown" of precipitation in the tropics (Andersson et al., 2005). The Incremental Analysis Update adds analysis increments gradually through the analysis cycle. This approach reduces the spindown problem (Rienecker et al., 2011).

In addition to improvements to forecast models and data assimilation systems, investment has been made in the rescue, reprocessing and homogenization of conventional and satellite observations assimilated into forecast models. Expanded and improved observational databases better constrain analyses and improve forecasts (Brönnimann et al., 2018). A critical step in this direction is the reduction of nonclimatic changes that result from changes in the assimilation database, in particular as satellite sensors are decommissioned and new sensors come online. Biases of sensors also change over the lifetimes of satellites, which may introduce spurious trends if uncorrected. Changes in radiosonde instrument packages over time also introduce inhomogeneities into the observation stream. All modern reanalyses use Variational Bias Correction (VBC), an automated scheme that detects new satellite data streams, and develop continually adjusted estimates of bias corrections for radiances within the variational analysis system based on all available information. Corrections are estimated such that the inconsistencies between satellite and conventional observations are minimized (Dee et al., 2011). However, bias corrections may not be implemented in regions with few conventional observations, such as the Arctic, or for some satellite sensors and channels that negatively impact analyses. Details of how VBC is used differ between reanalyses. A key update for ERA5 over ERA-Interim is extending the VBC scheme to include ozone, aircraft, and surface pressure data. MERRA2 also uses a VBC scheme for aircraft temperatures (Gelaro et al., 2017). JRA55, on the other hand, does not use temperatures from aircraft (Kobayashi et al., 2015).

Sea ice and sea surface temperature, along with greenhouse gas concentrations and solar irradiance are generally prescribed boundary conditions. CFSR/CFSv2 is unique in that sea ice extent and thickness are prognostic variables. Predicted extent is updated using satellite-derived estimates of ice concentration. While several different passive microwave sea ice retrieval algorithms are in use (Andersen et al., 2007; Comiso et al., 2017), they all use similar data. However, reanalyses differ in how sea ice data are used. ERA-Interim and ERA5 set grid cells with concentrations less than 20% to open ocean and use a fractional concentration for grid cells greater than 20%. JRA-55 uses a binary classification of grid cells (100% ice-covered or open ocean) with a 55% concentration threshold (Kobayashi et al., 2015). MERRA and MERRA2 use a 50% concentration threshold, whereas CFSR/CFSv2 use a 15% threshold. These differences can be important because a sea ice cover significantly reduces ocean-atmosphere exchange of sensible heat and water vapor and causes a marked change in surface albedo. Most reanalyses, with the exception of MERRA, which uses a fixed albedo, include seasonally varying albedo.

The reanalysis data were downloaded at 3-h or 6-h time resolutions depending on the reanalysis. Daily precipitation totals were calculated and then regridded to a 50 km Equal Area Scalable Earth grid version 1.0 (Brodzik & Knowles, 2005) using ESMPy tools (https://www.earthsystemcog.org/projects/esmpy/). Monthly statistics were then generated from regridded precipitation fields. Sources for reanalyses and respective time resolutions are given in Table 1. A 50-km resolution was chosen because it best matched the spatial resolutions for archived reanalysis data.

2.2. Arctic Drifting Stations

As already introduced, direct measurements of precipitation over the Arctic Ocean are sparse. Even today, much of our information comes from the Russian NP drifting stations maintained by the Arctic and Antarctic Research Institute. The first ice station was established in 1937 (NP-1). Observations were interrupted by World War II, and then the program resumed in 1950 (NP-2) and lasted until 1991 (NP-30 and NP-31). It resumed again in 2003–2004 with the establishment of NP-32 and NP-33. Here we use data from eight stations (NP22 and NP-24 to NP-31) that have observations for the 1979–1991 period and for which gauge corrections have been applied (see below). These data were obtained from the "Arctic Ocean Snow

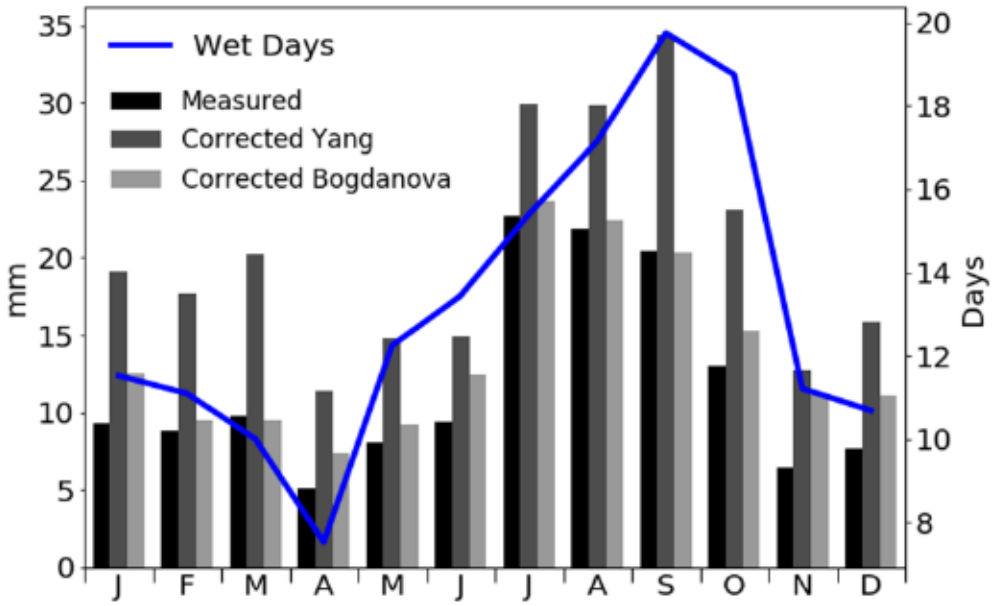

Figure 3. Climatologies of measured and bias-adjusted monthly precipitation, and mean number of wet days from North Pole drifting stations. Bias-adjusted data are from Yang (1999) and Bogdanova et al. (2002). Wet days are the number of days with precipitation of at least 1 mm.

and Meteorological Observations from Drifting Stations 1937, 1950–1991" data set published by the National Snow and Ice Data Center. Up until NP-24, drifting station locations were recorded every 3 h by terrestrial astronomical observations when weather conditions permitted. Starting with NP-25, locations were determined by satellite-based navigation. The NP sites provide measurements of both precipitation (including amount, occurrence, and phase) and snow cover (the latter from manual surveys) that are mostly representative of the central Arctic Ocean and provide little coastal information (Webster et al., 2014) (Figure 1). Precipitation and snow observations from this data set have been summarized by Warren et al. (1999), Yang (1999), Bogdanova et al. (2002), and Colony et al. (1998). Daily present weather reports from the NP sites included in the Advanced Comprehensive Ocean-Atmosphere Data Set (Woodruff et al., 1987) were used by Clark et al. (1996) and Serreze et al. (1997) in a study of spatial and seasonal variations in precipitation frequency, phase, and intensity across the Arctic Ocean.

Gauge measurements are prone to error in the northern environment. Wind-induced undercatch of snowfall has long been recognized as a problem. Errors may also be introduced by evaporation from gauges, condensation on the inside of gauges, adherence of water on the gauge material after the gauge is emptied (known as "wetting losses"), and neglect of trace precipitation and false precipitation resulting from blowing snow from the surface falling into gauges (Golubev et al., 1999; Sevruk & Hamon, 1984). Nevertheless, the NP records represent the best data source available to validate the reanalysis precipitation output.

Two correction methods have been applied to the NP precipitation records. Yang (1999) applied the World Meteorological Organization Organizing Committee correction method to daily NP observations collected between 1957 and 1991. The correction factors (multipliers to the raw data) have a mean of 1.71 and a maximum of 1.93. Bogdanova et al. (2002) applied the method derived by Golubev et al. (1999) to the same daily data set, yielding correction factors with a mean of 1.28 and maximum of 1.51. The key difference is that the World Meteorological Organization wind corrections are only applied for wind speeds less than 6.5 m/s. The adjusted annual mean precipitation from Yang (1999) is 256 mm, compared to 165 mm from Bogdanova et al. (2002). Bogdanova et al. (2002) argue that the Yang (1999) estimates are too high, given persistent stable anticyclonic conditions, low air temperatures, and low water vapor content over the Arctic Ocean for much of the year. They suggest that the overestimation of precipitation results from neglecting false precipitation blown into the gauge from surrounding snow surfaces during blizzards and strong wind events.

Figure 3 shows the "raw" mean monthly precipitation from the NP records for the period 1979–1991 along with adjusted values from both Yang (1999) and Bogdanova et al. (2002) and the number of wet days from

Yang (1999). For the Tretyakov gauges used at the drifting station, precipitation amounts greater than 0.1 mm are considered measurable. Nonzero precipitation less than 0.1 mm is recorded as trace. From both adjusted data sets, the precipitation minimum (along with the number of wet days and days with measurable precipitation) occurs in April and there is a warm season maximum. The warm season precipitation maximum reflects both the higher levels of atmospheric water vapor and the summer maximum in the influx of extratropical cyclones into the central Arctic Ocean (Serreze & Barry, 2014). However, the timing of maximum precipitation depends on the correction method applied to the NP data. There is a September maximum using the Yang (1999) approach and a July maximum using the Bogdanova et al. (2002) approach. Based on Bogdanova et al. (2002), precipitation is already declining by September. Wet days and the number of days with measurable precipitation peak in September. Measurable precipitation occurs 162 days a year (Yang, 1999), yet when records of trace precipitation are included, nonzero precipitation occurs on average 351 days a year. Bogdanova et al. (2002) by comparison identify an average of 243.5 nonzero precipitation days. An obvious conclusion is that while validation of precipitation from the reanalyses is challenged by sparse observations over the Arctic Ocean, there is considerable uncertainty in the observations themselves. One area of universal agreement is that the majority of precipitation events occur as solid precipitation. However, liquid precipitation has been reported in all months. Based on the present weather codes in the Advanced Comprehensive Ocean-Atmosphere Data Set records through 1991 (Serreze et al., 1997), as much as 50% of precipitation events at the NP sites in July can occur as liquid precipitation, with about 30% occurring as liquid precipitation in June and August. Given the warming Arctic environment, these figures have probably changed.

We use both gauge-corrected data sets to evaluate the reanalysis precipitation estimates. We do so in two ways. First, we compare annual and monthly means aggregated over all of the NP locations with the reanalysis values aggregated over the Arctic Ocean domain shown in Figure 1. As can be seen, NP drifting stations visited much of the central Arctic Ocean but did not visit the Barents or Kara Seas. Our Arctic Ocean domain, therefore, differs from that used in other papers (e.g., Serreze et al., 2006) by eliminating these regions. Second, we compare total precipitation from a given year and month from individual NP stations with the reanalysis precipitation following station trajectories. These annual and monthly time series of reanalysis precipitation are calculated by aggregating daily precipitation from grid cells corresponding to daily locations of drifting stations.

3. Results

3.1. Differences Between Reanalyses

We start by looking at monthly mean precipitation rates (millimeter per day) averaged over the Arctic Ocean domain and contrast these with global mean rates (Figure 4). Both the global and Arctic Ocean time series have been smoothed with a 12-month moving average to remove seasonal variations. As reported elsewhere (e.g., Bosilovich et al., 2015, 2017; Gelaro et al., 2017), global mean precipitation rates from reanalyses show some nonphysical variations introduced by changes in the observational database. Of note is the jump in global MERRA precipitation starting in 1998 related to the introduction of Advanced TIROS Operational Vertical Sounder and increased precipitation in ERA-Interim attributed to the loss of Special Sensor Microwave/Imager platforms F13, F14, and F15 in the late 2000s (Bosilovich et al., 2017). For the Arctic Ocean domain, these nonphysical variations are not visible and may simply be hidden by the pronounced interannual variations resulting from averaging over a smaller region.

There are obvious differences in precipitation amounts for both domains. Focusing on the Arctic Ocean, CFSR and MERRA2 are clearly the wettest, especially in the early part of the record, while MERRA is the driest. MERRA2 is wetter by 0.23 mm per day than its predecessor MERRA based on the mean of monthly precipitation rates for the 1980–2015 period common to both products. While tracking down causes of differences between reanalyses is challenging given the complexity of model and assimilation systems, a fundamental change that may bear on the difference is that MERRA2 places constraints on total atmospheric mass, forcing global precipitation, and evaporation rates to be essentially the same (Takacs et al., 2016). Despite differences in precipitation amount, the reanalyses show similar patterns of interannual variability, and the time series are well correlated: correlation coefficients for time series of annual total precipitation range from a low of 0.67 (between MERRA2 and ERA-Interim) to 0.95 (ERA-Interim and JRA55). None

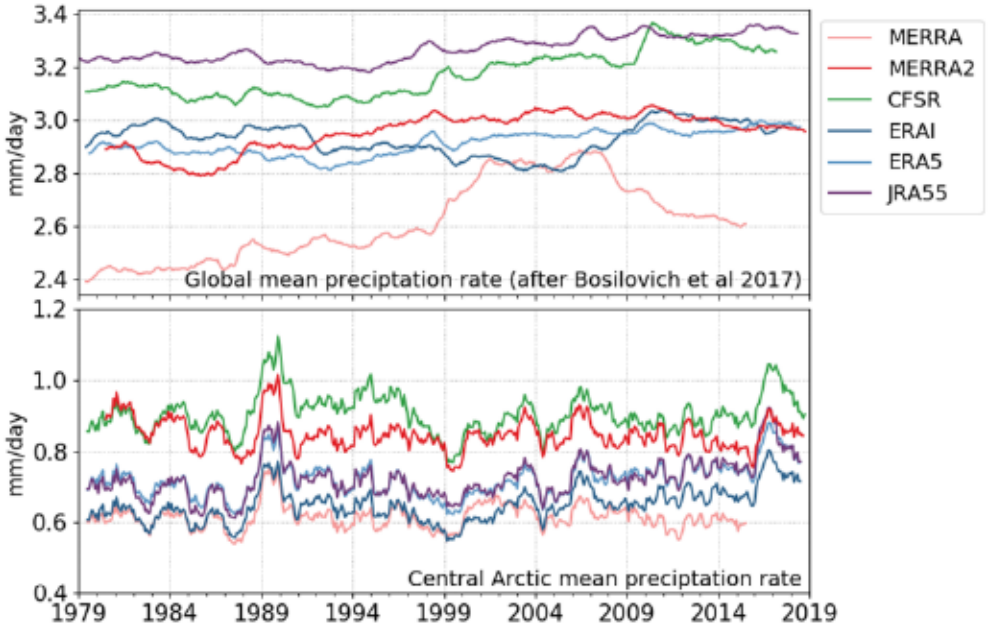

Figure 4. Mean precipitation rates (millimeter per day) for the reanalyses used in this study for the globe (top) and the Arctic Ocean domain (bottom).

of the reanalyses shows obvious evidence of long-term trends in precipitation, and all of the reanalyses show high precipitation amounts in 1989, 1990, 1995, and 2017 over the Arctic Ocean.

Figure 5 provides a breakdown of precipitation for different regions of the Arctic Ocean (see Figure 1), accumulated from 1 August through 30 April, spanning the sea ice growth season and the snow accumulation period. Regions are defined following Meier et al. (2007). The 1 August start is chosen to include early sea ice growth, while the 30 April end is chosen to include the March sea ice extent maximum. The conclusions from Figure 4 of similar patterns of interannual variability hold at the regional scale, which is very encouraging. Again, MERRA2 and CFSR emerge as the two "wet" reanalyses.

In Figure 6, we plot mean seasonal cycles of precipitation from the NP records along with mean seasonal cycles from the reanalyses, calculated using precipitation from the grid cells corresponding to the daily locations of the NP stations. Qualitatively consistent with the NP records, all of the reanalyses depict a cold season minimum and a late summer to early autumn maximum in precipitation. There are again differences in precipitation amount, with the two "wet" reanalyses (CFSR and MERRA2) seen in the annual means (Figures 4 and 5) also wet during the cold season. MERRA2 is similar to ERA5, ERA-Interim, and JRA55 during the warm months. We will examine biases with respect to the NP records later, but it is obvious from Figure 6 that apart from MERRA, the reanalyses are high during summer compared to observations, even with respect to the Yang (1999) record with its larger gauge adjustments. During winter, reanalysis values are reasonably close to those from Yang (1999). As assessed over the Arctic Ocean domain (not shown), seasonal cycles of precipitation from the reanalyses are smoother than seen in Figure 6, as expected from averaging over a larger area with many more data values.

Statistical distributions of daily precipitation totals as cumulative distribution functions (CDFs) over the snow accumulation period for each reanalysis follow in Figure 7. Each CDF is estimated by binning (into 0.1-mm bins) daily precipitation greater than zero for each day from 1980 through 1990 for every 50-km grid cell corresponding to the daily location of a drifting station. In analyses of daily total precipitation for the globe as a whole, daily totals less than 1 mm are typically considered drizzle (e.g. Sun et al., 2006). Daily totals greater than 1 mm and less than 10 mm are considered light precipitation, whereas daily totals greater than 10 mm are considered heavy precipitation. Recall that, in this study, we define days with more than 1 mm as wet days. Figure 7 only shows bins for daily total precipitation less than 6 mm, the intent being to focus on differences between the reanalyses in drizzle and lighter precipitation. Between 76% (CFSR/

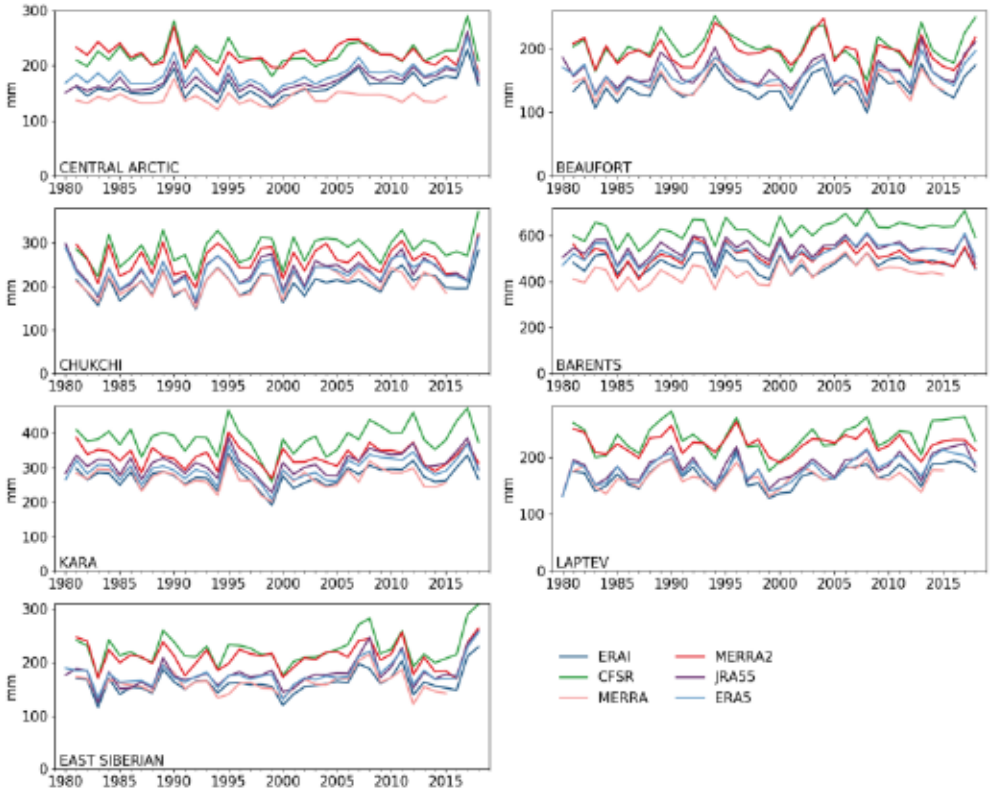

Figure 5. 1 August to 30 April total precipitation for Arctic Ocean regions.

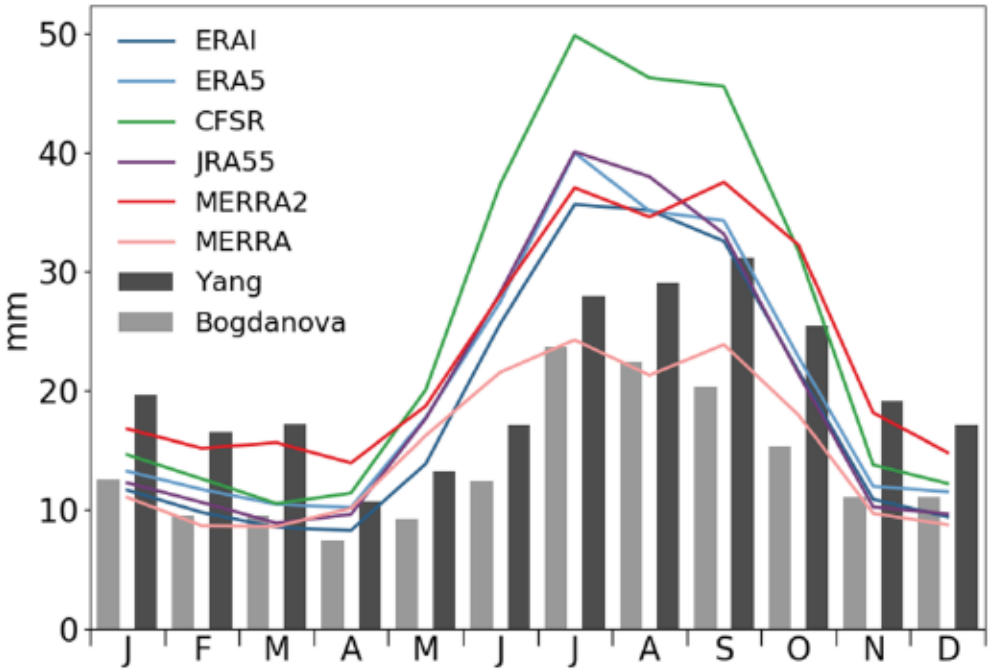

Figure 6. Mean seasonal cycles of bias-adjusted monthly precipitation from Yang (1999) and Bogdanova et al. (2002) and from the different reanalyses. Reanalysis precipitation climatologies are calculated using daily total precipitation from grid cells corresponding to daily locations of NP drifting stations.

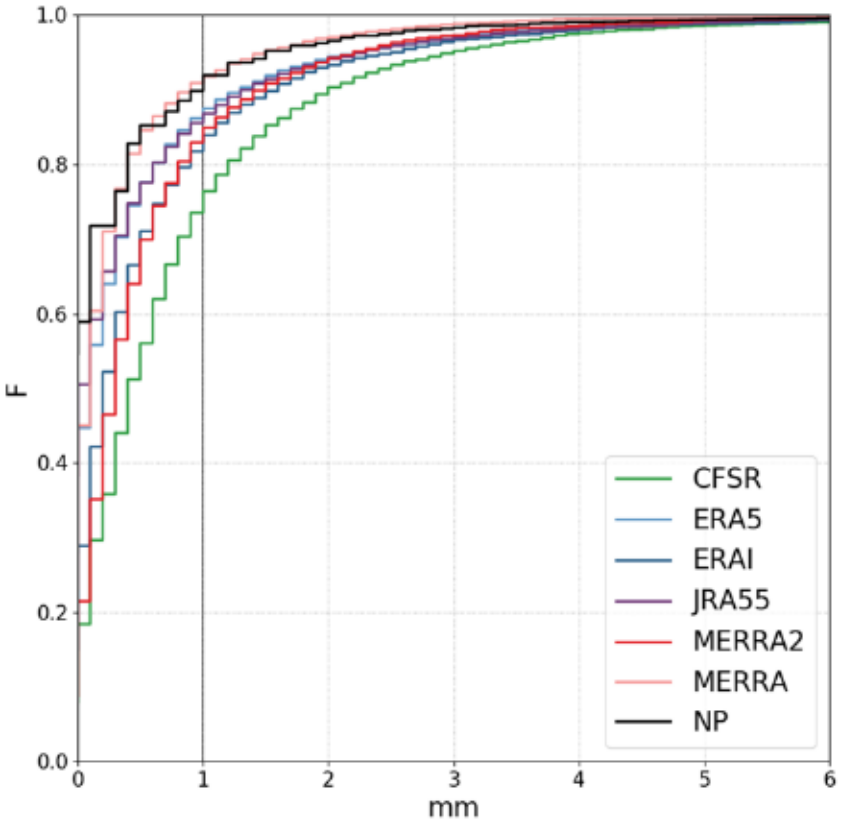

Figure 7. Cumulative distribution functions (CDFs) of daily total precipitation for grid cells corresponding to locations of North Pole drifting stations from 1 August through 30 April. North Pole (NP) drifting station data are from Yang (1999). Bins greater than 6 mm are not shown to focus on drizzle and light precipitation.

CFSv2) and 92% (MERRA) of daily precipitation events in the reanalyses represent drizzle. In terms of precipitation amount, drizzle (in general, very light snowfall) accounts for between 34% (CFSR/CFSv2) and 55% (MERRA) of total precipitation. Heavy precipitation (daily precipitation >10 mm) is between 0.5% (MERRA) and 2.7% (JRA55). The largest differences between CDFs are for drizzle. Although differences persist into the light precipitation range, they diminish for larger daily precipitation events, becoming negligible for heavy precipitation fractions. The CDF of nonzero precipitation for the NP stations indicates that as much as 92% of days with precipitation have daily precipitation amounts less than 1 mm, contributing 42% of the total observed precipitation amount. This indicates that the size distribution of daily precipitation events represented in the reanalyses is similar to that seen in observations. Note that CFSR/CFSv2 and MERRA2 have the lowest cumulative frequencies for precipitation amounts less than 6 mm. This is not inconsistent with these reanalyses having the highest monthly, seasonal, and annual total precipitation because low frequencies of drizzle and light events mean that these reanalyses have a greater number of heavier events. CDFs computed for individual months (not shown) are overall quite similar to those based on aggregating data from 1 August to 30 April. Notably, while daily precipitation amounts are highest in late summer and early autumn in both the reanalyses and in the observations, the contributions to total precipitation from small (less than 1 mm) events are on average only 10% lower in this same period than during winter months. Results are similar when the analysis is performed for the full Arctic Domain and for regions within this domain (not shown).

We next examine time series of total precipitation for the Arctic Ocean domain along with the totals from drizzle events (< 1 mm) and wet days (anything ≥1 mm) for the 1 August to 30 April period (Figure 8). Results for total precipitation reflect those shown in Figure 4. Reanalyses fall into two clear groups: CFSR/CFSv2 and MERRA2, clearly the "wet" reanalyses produce on average 50 mm more precipitation over the course of the season than ERA-Interim, ERA5, MERRA, and JRA55. However, MERRA2 appears to

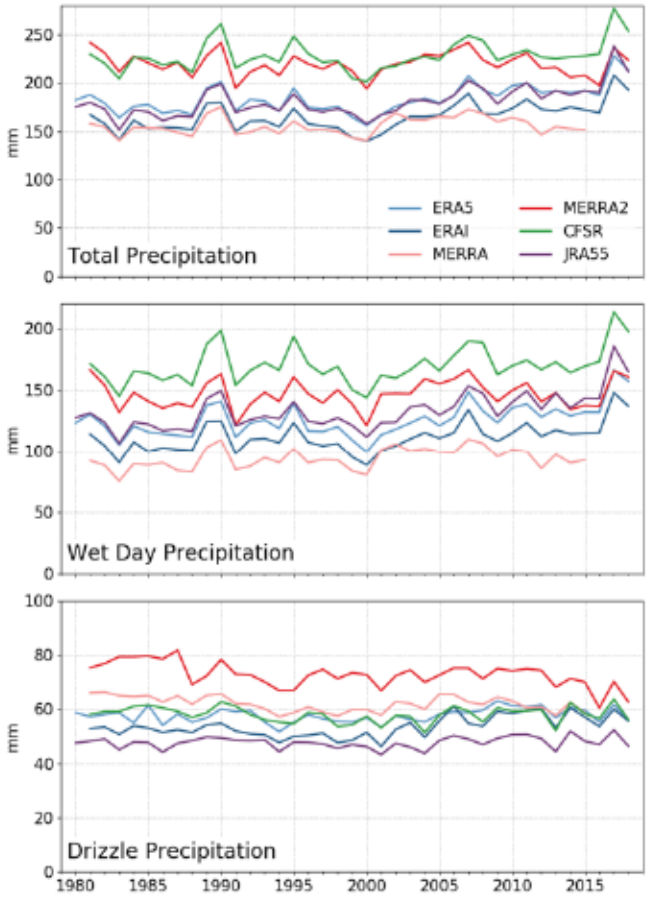

Figure 8. Total precipitation, wet day precipitation ($P \geq 1$ mm), and drizzle precipitation ($P < 1$ mm) for the Arctic Ocean domain.

converge toward ERA-Interim, ERA5, MERRA, and JRA55 in the last few years of the record. This was also noted by Stroeve et al. (submitted to JGR-Oceans) when comparing estimates of total snow volume from MERRA2 and ERA-Interim. Compared to the other reanalyses, total precipitation in CFSR/CFSv2 involves a higher contribution from wet day events. However, CFSR/CFSv2 produces similar amounts of drizzle to ERA-Interim and ERA5. By contrast, MERRA2 produces larger amounts of both drizzle and wet day precipitation. JRA55 produces lower amounts of drizzle than other reanalyses but similar wet day precipitation to ERA5 and ERA-Interim.

Spatial patterns of total precipitation from 1 August through 30 April (Figure 9) are broadly similar for all reanalyses and capture the known basic pattern of Arctic precipitation. Key features are a dry central Arctic Ocean and Canadian Arctic Archipelago (Polar Desert) and a much wetter North Atlantic sector that extends into the Barents and Kara Seas, reflecting the influence of the Icelandic Low and the poleward terminus of the North Atlantic cyclone track. CFSR/CFSv2 and MERRA2 stand out as between 45 and 65 mm wetter over the Eurasian side of the Arctic Ocean and over parts of the Beaufort Sea. CFSR/CFSv2 also has noisy speckled patterns of precipitation over northern North America and Eurasian land masses suggestive of topographic influences. Spatial patterns of drizzle precipitation are very similar between the products in a qualitative sense, but MERRA2 stands out with distinctly higher drizzle totals over the Arctic Ocean, and a likely spurious region of especially high drizzle amounts over the Canadian Arctic Archipelago (supporting information Figure S1). Patterns of the frequencies of wet days show some differences (Figure 10) with the CFSR/CFSv2 and MERRA2 products having a high frequency of wet days over the eastern Arctic.

3.2. Comparisons With the NP Records

Figure 11 shows the annual time series of total precipitation from the reanalyses and annual total precipitation estimated using bias-adjusted precipitation from both Yang (1999) and Bogdanova et al. (2002) for the 1980–1990 period. Annual precipitation from the reanalyses was calculated by extracting precipitation from the reanalysis grid cell closest to the location of drifting stations for each day the drifting stations were in operation. Vertical bars to the right of the plot show the range and mean of the reanalysis and gauge precipitation for the 1980–1990 period. When compared to the adjusted precipitation from Yang (1999), reanalyses fall within the observed range. When compared with precipitation from Bogdanova et al. (2002) that has smaller corrections factors, reanalyses have too much precipitation in most years, with the exception of MERRA. The results are very similar when the mean annual total precipitation for the Arctic Domain is compared to the drifting station averages.

Monthly total precipitation expressed as percent biases with respect to the NP values from Yang (1999) follows in Figure 12. As already discussed, all reanalyses capture the basic seasonal cycle of precipitation from the gauge-based observations, with low precipitation in the cold season and maximum precipitation during summer and early autumn. Overall, percent differences between reanalysis estimates and the Yang (1999) observations are smallest in winter months when precipitation is also lowest and are largest during summer when precipitation is highest. This is important given that sea ice thickness retrievals from radar altimetry can only be achieved during the cold season. Recall from Figure 6, ERA-Interim, CFSR, and MERRA are close to the Bogdanova et al. (2002) estimates between November and March (not shown), and smaller than the Yang (1999) estimates in April, May, September, and October. Values from CFSR and MERRA2 (the wet reanalyses) by contrast exceed values depicted by Bogdanova et al. (2002) but are smaller than those depicted by Yang (1999) between November and March. Between July and August, only MERRA is close to observations, whereas all other reanalyses exceed observations, with CFSR having the largest bias.

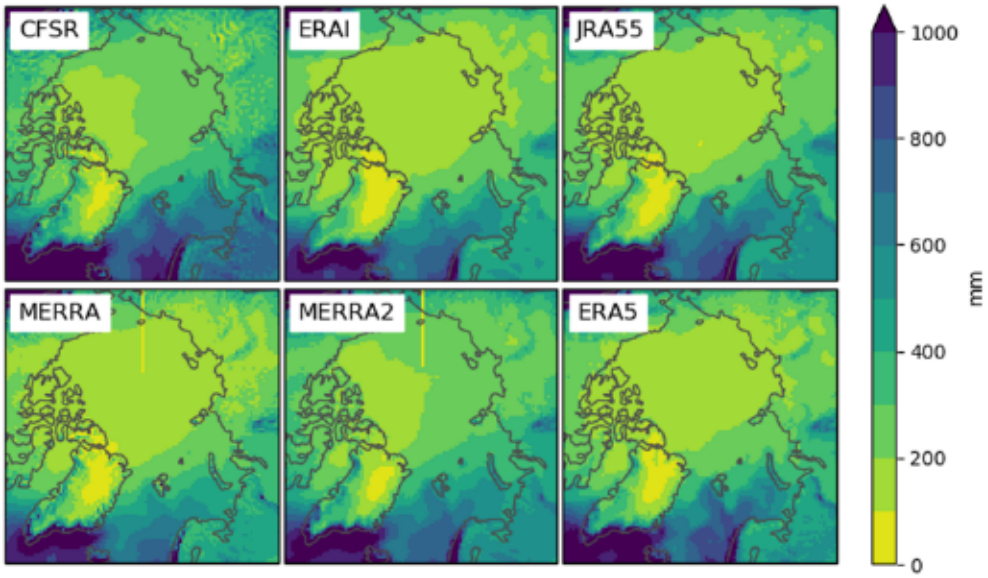

Figure 9. Total precipitation (millimeter) from August to April for the six reanalyses.

Correlations, mean biases, and root-mean-square errors for monthly total precipitation from the reanalyses and NP observations from Yang (1999) follow in Table 2. The reanalysis values are for the grid cells corresponding to the daily NP locations. Results are given for the August to April period and for the full year. Mean bias is the ratio of the mean of reanalysis precipitation to the mean observed corrected precipitation from Yang (1999). All correlations are broadly similar, though ERA5 has the highest correlation with observations for both the August to April period (0.64) and for the full year (0.62). The ERA5 bias for the August to April period is small (0.8 mm) and 1.0 mm for the annual period. For the August to April period, correlations for the other reanalyses are between 0.58 and 0.64. The RMSEs are between 12 and 15 mm. Metrics for the full year are very similar. Metrics for individual seasons are given in Table S1. Because more than one drifting station could be in operation at a given time, there can be more than 10 data points for any 1 month.

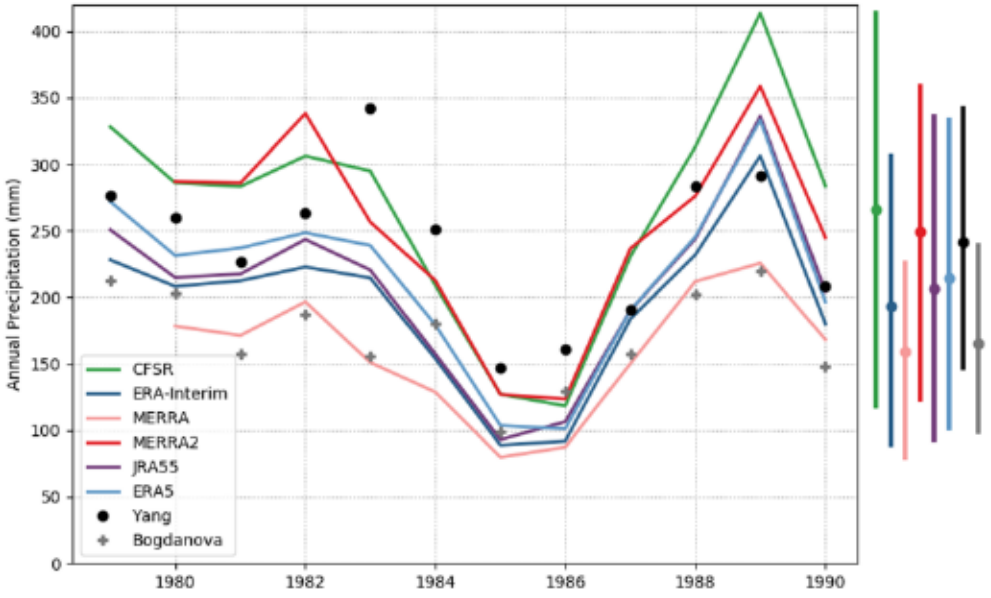

Figure 10. Wet day ($P \geq 1$ mm) precipitation frequency (as a fraction of all days) for the six reanalyses from August through April.

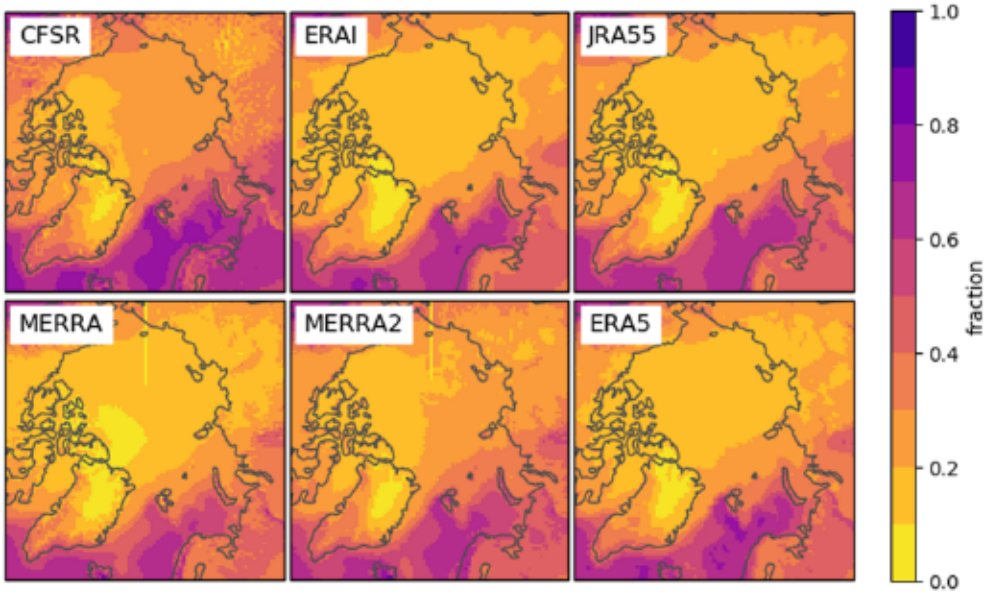

Figure 11. Annual total precipitation for the Arctic Ocean domain from the reanalysis and bias-adjusted precipitation from the North Pole Drifting Stations from Yang (1999) and Bogdanova et al. (2002). Vertical bars on the right show the mean (dot) and range (length of bar) of reanalysis and gauge precipitation for the 1980 to 1990 period.

Nevertheless, metrics for seasons are based on a small number of observations and should be viewed with appropriate caveats. Winter months have the lowest correlations but the smallest biases, while summer months have the highest correlation and also the largest biases. Autumn has both high correlations and small biases. The higher correlations in summer and autumn may be in part a statistical artifact resulting from summer having a larger spread of precipitation totals. For example, a 10-mm bias for a summer month in which observed precipitation is 50 mm still registers as a large event in the reanalysis record, whereas a 10

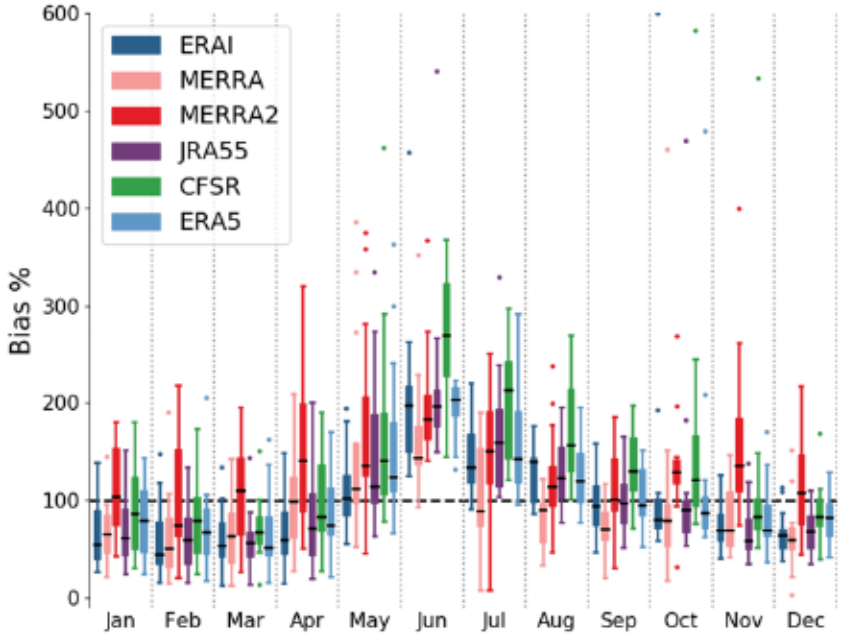

Figure 12. Monthly total precipitation expressed as biases with respect to the North Pole precipitation values from Yang (1999). Box and whiskers show the distribution of biases: boxes show the interquartile range, whiskers show the 10th and 90th percentiles, and horizontal black bars show the mean bias.

Table 2
Correlation Coefficients, Bias, and Root-Mean-Square Error (RMSE) Between Monthly Total Precipitation From the Reanalyses and North Pole Drifting Stations From Yang (1999) for the 1 August to 30 April Snow Accumulation Period and Annual Time Periods

Reanalysis	1 August to 30 April period			Annual		
	Correlation	Bias	RMSE (mm)	Correlation	Bias	RMSE
CFSR/CFSv2	0.62	1.0	14.2	0.59	1.2	16.1
ERA5	0.64	0.8	12.6	0.62	1.0	12.8
ERA-Interim	0.63	0.8	13.4	0.62	0.9	12.8
JRA55	0.62	0.8	13.6	0.59	0.9	13.9
MERRA	0.58	0.6	14.8	0.54	0.7	13.8
MERRA2	0.62	1.0	12.3	0.62	1.1	13.0

Note. Reanalysis precipitation is derived from daily total precipitation for the grid cells containing the daily locations of the NP stations.

mm bias for a winter month in which observed precipitation is 20 mm reduces or increases the observed precipitation event more. We also stress that our assessments are comparing precipitation at a point against precipitation at the grid cell level that represents a larger area.

4. Discussion and Conclusions

In terms of total annual precipitation over the Arctic Ocean domain and for different Arctic Ocean subregions, the time series from the reanalysis correlate fairly well, that is, interannual variability is fairly consistent among them. While certainly encouraging, this agreement is to be expected given that reanalyses use similar observational databases. However, the precipitation totals themselves show a large spread, largest in early autumn. MERRA2 and CFSR are the two wettest reanalyses, whereas JRA55 is the driest. While all of the reanalyses capture the basic spatial patterns of Arctic precipitation as they are known, there are also large differences in amount between them on the regional scale.

Since most precipitation over the Arctic Ocean falls as snow, the large differences in precipitation imply large differences in the mass of snow on sea ice that the reanalysis would depict. This has direct relevance to satellite retrievals of sea ice thickness from radar or laser altimetry. Differences are smallest in winter, the time of the year for which current radar altimetry sea ice thickness products are available. However, a seemingly small 10- to 20-cm difference in snow depth (corresponding to differences in precipitation in the range of 3.5–7.0 cm assuming a snow density of 350 km/m^3) can have a large impact on the total ice thickness retrieved. Stroeve and Notz (2018) report that a 10- to 20-cm difference in snow depth results in a 50- to 100-cm difference in ice thickness. Further, differences in snow depth will have a large impact on thermodynamic ice growth. The conductive heat flux through sea ice from the ocean to the atmosphere is a function of the conductivity of the snow and ice cover, as well as the thickness of the snow and ice. Snow conductivity is about 7 times smaller than that for sea ice; thus, a 20-cm snow layer can reduce the conductive heat flux by more than 50%, reducing thermodynamic ice growth. However, this may be countered by delayed autumn ice formation, linked in part to the higher internal energy of the upper ocean at summer's end. With delayed ice formation, there is less time for snow to accumulate on the ice, which by itself will foster more rapid ice growth. Smaller snow depths will also reduce the occurrence of submerged ice in areas of high accumulation, preventing flooding of the ice surface and formation of snow-ice.

Observations and the reanalyses indicate that between 76% and 92% of days with precipitation over the Arctic Ocean represent events less than 1 mm. These events, in turn, account for between 34% and 55% of the total annual precipitation. Some studies using reanalysis data (e.g., Boisvert et al., 2018) have ignored this light precipitation. Such an approach may be justified on a global scale in light of the tendency for climate models to produce overly frequent drizzle events (e.g., Dai, 2006; Pendergrass & Hartmann, 2014). However, given the significance of small events on Arctic Ocean totals in both observations and reanalyses, discarding drizzle may be the wrong approach. The prevalence of drizzle also complicates precipitation observations as do measurement errors, in particular those resulting from wind-induced turbulence (Sevruk et al., 1989).

Given the large spread in precipitation estimates between the reanalyses, the obvious question arises as to which one performs best. The conundrum is that while the use of reanalyses is in large part motivated by the paucity of observations, it is only with the sparse observations that the question can be answered. And it is not simply that the precipitation observations are sparse—they are strongly influenced by gauge undercatch and other problems. The two methods that have been applied to the NP data yield very different results.

From an assessment of correlations with the NP records, bias with respect to these records, and the consistency between the reanalyses in terms of spatial patterns of precipitation and interannual variability, all of the reanalyses examined here appear to be of roughly equal value for supporting retrievals of ice thickness. However, this assumes that one can have confidence in bias corrections that would have to be applied to the reanalysis data, which goes right back to the issue that bias adjustments to the observations are themselves uncertain. However, only CFSR, MERRA2, JRA55, and ERA-5 will continue to be produced beyond 2019. Given that the native resolution of ERA5 is high, and that it is likely to be continued into the foreseeable future, we argue that ERA5 will best serve as the basis of schemes to obtain snow mass atop sea ice to enable improved retrievals of sea ice thickness from satellite data.

Acknowledgments
This study was supported by NASA grant NNX16AK85G and NSF grants PLR 1603914, OPP 1748953, and ICER 1918230. MERRA and MERRA2 data were retrieved from NASA Goddard Earth Sciences Data and Information Services Center (https://disc.gfsc.nasa.gov). CFSR/CFSv2 and JRA55 data were retrieved from NCAR Research Data Archive (https://rda.ucar.edu). ERA-Interim was retrieved from the European Center for Medium Range Weather Forecasts (ECMWF) (https://www.ecmwf.int). ERA5 data were retrieved from Copernicus Climate Change Service (C3S) (https://cds.climate.copernicus.eu). North Pole drifting station precipitation and drift trajectories were obtained from the "Arctic Ocean Snow and Meteorological Observations from Drifting Stations 1937, 1950–1991" data set published by the National Snow and Ice Data Center (NSIDC).

References

Andersen, S., Tonboe, R., Kaleschke, L., Heygster, G., & Pedersen, L. T. (2007). Intercomparison of passive microwave sea ice concentration retrievals over the high-concentration Arctic sea ice. *Journal of Geophysical Research*, *112*, C08004. https://doi.org/10.1029/2006JC003543

Andersson, E., Bauer, P., Beljaars, A., Chevallier, F., Hólm, E., Janisková, M., et al. (2005). Assimilation and modeling of the atmospheric hydrological cycle in the ECMWF forecasting system. *Bulletin of the American Meteorological Society*, *86*(3), 387–402. https://doi.org/10.1175/BAMS-86-3-387

Bogdanova, E. G., Ilyin, B. M., & Dragomilova, I. V. (2002). Application of a comprehensive bias-correction model to precipitation measured at Russian North Pole drifting stations. *Journal of Hydrometeorology*, *3*(6), 700–713. https://doi.org/10.1175/1525-7541(2002)003<0700:AOACBC>2.0.CO;2

Boisvert, L. N., Webster, M. A., Petty, A. A., Markus, T., Bromwich, D. H., & Cullather, R. I. (2018). Intercomparison of precipitation estimates over the Arctic Ocean and its peripheral seas from reanalyses. *Journal of Climate*, *31*(20), 8441–8462. https://doi.org/10.1175/JCLI-D-18-0125.1

Bosilovich, M. G., Chern, J.-D., Mocko, D., Robertson, F. R., & da Silva, A. M. (2015). Evaluating observation influence on regional water budgets in reanalyses. *Journal of Climate*, *28*(9), 3631–3649. https://doi.org/10.1175/JCLI-D-14-00623.1

Bosilovich, M. G., Robertson, F. R., & Chen, J. (2011). Global energy and water budgets in MERRA. *Journal of Climate*, *24*(22), 5721–5739. https://doi.org/10.1175/2011JCLI4175.1

Bosilovich, M. G., Robertson, F. R., Takacs, L., Molod, A., & Mocko, D. (2017). Atmospheric water balance and variability in the MERRA-2 reanalysis. *Journal of Climate*, *30*(4), 1177–1196. https://doi.org/10.1175/JCLI-D-16-0338.1

Brodzik, M. J., & Knowles, K. W. (2005). Chapter 5: EASE-Grid: A versatile set of equal-area projections and grids. In M. F. Goodchild (Ed.), *Discrete global grids: a web book* (pp. 98–113). National Center for Geographic Information and Analysis. Santa Barbara, California USA. Retrieved from https://escholarship.org/uc/item/9492q6sm

Brönnimann, S., Allan, R., Atkinson, C., Buizza, R., Bulygina, O., Dahlgren, P., et al. (2018). Observations for reanalyses. *Bulletin of the American Meteorological Society*, *99*(9), 1851–1866. https://doi.org/10.1175/BAMS-D-17-0229.1

Clark, M. P., Serreze, M. C., & Barry, R. G. (1996). Characteristics of Arctic Ocean climate based on COADS data, 1980–1993. *Geophysical Research Letters*, *23*(15), 1953–1956. https://doi.org/10.1029/96GL01807

Colony, R., Radionov, V., & Tanis, F. J. (1998). Measurements of precipitation and snow pack at Russian North Pole drifting stations. *Polar Record*, *34*(188), 3. https://doi.org/10.1017/S0032247400014923

Comiso, J. C., Meier, W. N., & Gersten, R. (2017). Variability and trends in the Arctic Sea ice cover: Results from different techniques: Trends in the arctic sea ice cover. *Journal of Geophysical Research: Oceans*, *122*, 6883–6900. https://doi.org/10.1002/2017JC012768

Cullather, R. I., & Bosilovich, M. G. (2011). The moisture budget of the polar atmosphere in MERRA. *Journal of Climate*, *24*(11), 2861–2879. https://doi.org/10.1175/2010JCLI4090.1

Dai, A. (2006). Precipitation characteristics in eighteen coupled climate models. *Journal of Climate*, *19*(18), 4605–4630. https://doi.org/10.1175/JCLI3884.1

Dee, D. P., Uppala, S. M., Simmons, A. J., Berrisford, P., Poli, P., Kobayashi, S., et al. (2011). The ERA-Interim reanalysis: Configuration and performance of the data assimilation system. *Quarterly Journal of the Royal Meteorological Society*, *137*(656), 553–597. https://doi.org/10.1002/qj.828

Ebert, E. E., & Curry, J. A. (1993). An intermediate one-dimensional thermodynamic sea ice model for investigating ice-atmosphere interactions. *Journal of Geophysical Research*, *98*(C6), 10,085–10,109. https://doi.org/10.1029/93JC00656

Fujiwara, M., Wright, J. S., Manney, G. L., Gray, L. J., Anstey, J., Birner, T., et al. (2017). Introduction to the SPARC Reanalysis Intercomparison Project (S-RIP) and overview of the reanalysis systems. *Atmospheric Chemistry and Physics*, *17*(2), 1417–1452. https://doi.org/10.5194/acp-17-1417-2017

Gelaro, R., McCarty, W., Suárez, M. J., Todling, R., Molod, A., Takacs, L., et al. (2017). The Modern-Era Retrospective Analysis for Research and Applications, Version 2 (MERRA-2). *Journal of Climate*, *30*(14), 5419–5454. https://doi.org/10.1175/JCLI-D-16-0758.1

Giles, K. A., Laxon, S. W., Wingham, D. J., Wallis, D. W., Krabill, W. B., Leuschen, C. J., et al. (2007). Combined airborne laser and radar altimeter measurements over the Fram Strait in May 2002. *Remote Sensing of the Cryosphere Special Issue*, *111*(2-3), 182–194. https://doi.org/10.1016/j.rse.2007.02.037

Golubev, V. S., Konovalov, D. A., Simonenko, A. Y., & Tovmach, Y. V. (1999). Precipitation measurements correction and quality of corrected data from Valdai Hydrology Station data. *Russian Meteorology and Hydrology*, *1*, 65–74.

Grumbine, R. W. (1996). Automated sea ice concentration analysis. *MMAB Technical Note*, *120*, 13.

Huffman, G. J., Adler, R. F., Arkin, P., Chang, A., Ferraro, R., Gruber, A., et al. (1997). The Global Precipitation Climatology Project (GPCP) combined precipitation dataset. *Bulletin of the American Meteorological Society*, *78*(1), 5–20. https://doi.org/10.1175/1520-0477(1997)078<0005:TGPCPG>2.0.CO;2

Kobayashi, S., Ota, Y., Harada, Y., Ebita, A., Moriya, M., Onoda, H., et al. (2015). The JRA-55 reanalysis: General specifications and basic characteristics. *Journal of the Meteorological Society of Japan. Ser. II*, *93*(1), 5–48. https://doi.org/10.2151/jmsj.2015-001

Kwok, R. (2010). Satellite remote sensing of sea-ice thickness and kinematics: A review. *Journal of Glaciology*, *56*(200), 1129–1140.

Kwok, R., & Cunningham, G. F. (2008). ICESat over Arctic sea ice: Estimation of snow depth and ice thickness. *Journal of Geophysical Research*, *113*, C08010. https://doi.org/10.1029/2008JC004753

Lawrence, I. R., Tsamados, M. C., Stroeve, J. C., Armitage, T. W. K., & Ridout, A. L. (2018). Estimating snow depth over Arctic sea ice from calibrated dual-frequency radar freeboards. *The Cryosphere*, *12*(11), 3551–3564. https://doi.org/10.5194/tc-12-3551-2018

Lindsay, R., Wensnahan, M., Schweiger, A., & Zhang, J. (2014). Evaluation of seven different atmospheric reanalysis products in the Arctic. *Journal of Climate*, *27*, 2588–2606. https://doi.org/10.1175/JCLI-D-13-00014.1

Liston, G. E., Polashenski, C., Rösel, A., Itkin, P., King, J., Merkouriadi, I., & Haapala, J. (2018). A distributed snow-evolution model for sea-ice applications (SnowModel). *Journal of Geophysical Research: Oceans*, *123*, 3786–3810. https://doi.org/10.1002/2017JC013706

Markus, T., Massom, R., Worby, A., Lytle, V., Kurtz, N., & Maksym, T. (2011). Freeboard, snow depth and sea-ice roughness in East Antarctica from in situ and multiple satellite data. *Annals of Glaciology*, *52*(57), 242–248. https://doi.org/10.3189/172756411795931570

Matsumoto, T., Ishii, M., Fukuda, Y., & Hirahara, S. (2006). Sea ice data derived from microwave radiometer for climate monitoring. Presented at the AMS 14th Conference on Satellite Meteorology and Oceanography. Retrieved from https://ams.confex.com/ams/Annual2006/techprogram/paper_101105.htm

Meier, W. N., Stroeve, J., & Fetterer, F. (2007). Whither Arctic sea ice? A clear signal of decline regionally, seasonally and extending beyond the satellite record. *Annals of Glaciology*, *46*, 428–434. https://doi.org/10.3189/172756407782871170

Nandan, V., Geldsetzer, T., Yackel, J., Mahmud, M., Scharien, R., Howell, S., et al. (2017). Effect of snow salinity on CryoSat-2 Arctic first-year sea ice freeboard measurements. *Geophysical Research Letters*, *44*, 10,419–10,426. https://doi.org/10.1002/2017GL074506

Pendergrass, A. G., & Hartmann, D. L. (2014). Two modes of change of the distribution of rain. *Journal of Climate*, *27*(22), 8357–8371. https://doi.org/10.1175/JCLI-D-14-00182.1

Petty, A. A., Webster, M., Boisvert, L., & Markus, T. (2018). The NASA Eulerian Snow on Sea Ice Model (NESOSIM) v1.0: Initial model development and analysis. *Geoscientific Model Development*, *11*(11), 4577–4602. https://doi.org/10.5194/gmd-11-4577-2018

Rienecker, M. M., Suarez, M. J., Gelaro, R., Todling, R., Bacmeister, J., Liu, E., et al. (2011). MERRA: NASA's Modern-Era Retrospective Analysis for Research and Applications. *Journal of Climate*, *24*(14), 3624–3648. https://doi.org/10.1175/JCLI-D-11-00015.1

Rostosky, P., Spreen, G., Farrell, S. L., Frost, T., Heygster, G., & Melsheimer, C. (2018). Snow depth retrieval on arctic sea ice from passive microwave radiometers—Improvements and extensions to multiyear ice using lower frequencies. *Journal of Geophysical Research: Oceans*, *123*, 7120–7138. https://doi.org/10.1029/2018JC014028

Saha, S., Moorthi, S., Pan, H.-L., Wu, X., Wang, J., Nadiga, S., et al. (2010). The NCEP Climate Forecast System Reanalysis. *Bulletin of the American Meteorological Society*, *91*(8), 1015–1058. https://doi.org/10.1175/2010BAMS3001.1

Saha, S., Moorthi, S., Wu, X., Wang, J., Nadiga, S., Tripp, P., et al. (2013). The NCEP Climate Forecast System Version 2. *Journal of Climate*, *27*(6), 2185–2208. https://doi.org/10.1175/JCLI-D-12-00823.1

Serreze, M., & Barry, R. (2014). *The Arctic climate system. Cambridge Atmospheric and Space Science Series*. Cambridge: Cambridge University Press.

Serreze, M. C., Barrett, A. P., & Lo, F. (2005). Northern high-latitude precipitation as depicted by atmospheric reanalyses and satellite retrievals. *Monthly Weather Review*, *133*(12), 3407–3430. https://doi.org/10.1175/MWR3047.1

Serreze, M. C., Barrett, A. P., Slater, A. G., Woodgate, R. A., Aagaard, K., Lammers, R. B., et al. (2006). The large-scale freshwater cycle of the Arctic. *Journal of Geophysical Research*, *111*, C11010. https://doi.org/10.1029/2005JC003424

Serreze, M. C., Barrett, A. P., & Stroeve, J. (2012). Recent changes in tropospheric water vapor over the Arctic as assessed from radiosondes and atmospheric reanalyses. *Journal of Geophysical Research*, *117*, D10104. https://doi.org/10.1029/2011JD017421

Serreze, M. C., Maslanik, J. A., & Key, J. (1997). Atmospheric and sea ice characteristics of the Arctic Ocean and the SHEBA field region of the Beaufort Sea. NSIDC Special Report No. 4. Boulder, CO, USA: National Snow and Ice Data Center. Retrieved from https://nsidc.org/sites/nsidc.org/files/files/nsidc_special_report_4.pdf

Sevruk, B., & Hamon, W. R. (1984). International comparison of national precipitation gauges with a reference pit gauge. *WMO Instruments and Observing Methods Rep. No. 17*. World Meteorological Organization.

Sevruk, B., Hertig, I. A., & Spiess, R. (1989). Wind field deformation above precipitation gauge orifices. *IAHS Publication*, *179*, 65–70.

Stroeve, J., & Notz, D. (2018). Changing state of Arctic sea ice across all seasons. *Environmental Research Letters*, *13*(10), 103001. https://doi.org/10.1088/1748-9326/aade56

Sun, Y., Solomon, S., Dai, A., & Portmann, R. W. (2006). How often does it rain? *Journal of Climate*, *19*(6), 916–934. https://doi.org/10.1175/JCLI3672.1

Takacs, L. L., Suárez, M. J., & Todling, R. (2016). Maintaining atmospheric mass and water balance in reanalyses. *Quarterly Journal of the Royal Meteorological Society*, *142*(697), 1565–1573. https://doi.org/10.1002/qj.2763

Talagrand, O. (2010). Variational assimilation. In W. Lahoz, B. Khattatov, & R. Menard (Eds.), *Data assimilation: making sense of observations*, (pp. 41–67). Berlin, Heidelberg: Springer Berlin Heidelberg. https://doi.org/10.1007/978-3-540-74703-1_3

Walsh, J. E., & Chapman, W. L. (2001). 20th-century sea-ice variations from observational data. *Annals of Glaciology*, *33*, 444–448. https://doi.org/10.3189/172756401781818671

Warren, S. G., Rigor, I. G., Untersteiner, N., Radionov, V. F., Bryazgin, N. N., Aleksandrov, Y. I., & Colony, R. (1999). Snow depth on Arctic sea ice. *Journal of Climate*, *12*(6), 1814–1829. https://doi.org/10.1175/1520-0442(1999)012<1814:SDOASI>2.0.CO;2

Webster, M. A., Rigor, I. G., Nghiem, S. V., Kurtz, N. T., Farrell, S. L., Perovich, D. K., & Sturm, M. (2014). Interdecadal changes in snow depth on Arctic sea ice. *Journal of Geophysical Research: Oceans*, *119*, 5395–5406. https://doi.org/10.1002/2014JC009985

Woodruff, S. D., Slutz, R. J., Jenne, R. L., & Steurer, P. M. (1987). A comprehensive ocean-atmosphere data set. *Bulletin of the American Meteorological Society*, *68*(10), 1239–1250. https://doi.org/10.1175/1520-0477(1987)068<1239:ACOADS>2.0.CO;2

Yang, D. (1999). An improved precipitation climatology for the Arctic Ocean. *Geophysical Research Letters*, *26*(11), 1625–1628. https://doi.org/10.1029/1999GL900311